Journal of The Electrochemical Society, **165** (5) B227-B231 (2018)
0013-4651/2018/165(5)/B227/5/$37.00 © The Electrochemical Society

An Inkjet Printed Ti_3C_2-GO Electrode for the Electrochemical Sensing of Hydrogen Peroxide

Jiushang Zheng,[1] Jianglin Diao,[1] Yanzi Jin,[1,2] Ailing Ding,[1] Bin Wang,[1] Lizhou Wu,[2] Bo Weng,[1,z] and Jiucun Chen [1,3,z]

[1] *Institute for Clean Energy & Advanced Materials, Faculty of Materials and Energy, Southwest University, Chongqing 400715, People's Republic of China*
[2] *School of Chemistry and Chemical Engineering, Ankang University, Ankang 725000, People's Republic of China*
[3] *Key Laboratory of Luminescent and Real-Time Analytical Chemistry, Ministry of Education, College of Pharmaceutical Sciences, Southwest University, Chongqing 400715, People's Republic of China*

Novel two-dimensional Ti_3C_2 MXene nanosheets were successfully prepared by etching Al from Ti_3AlC_2 in LiF/HCl system. In order to further improve the dispersing property and electrical conductivity of Ti_3C_2 nanosheets, Ti_3C_2/graphene oxide (Ti_3C_2-GO) nanocomposites were synthesized and applied for the fabrication of inkjet-printed hydrogen peroxide (H_2O_2) sensor. The results of electrochemical characterization show that the prepared sensor maintains the biological activity of hemoglobin (Hb) and can be applied to the practical detection. The printed sensors display a dynamic range from 2 μM to 1 mM and a detection limit of 1.95 μM with a high sensitivity and excellent selectivity for H_2O_2 determination. Therefore, the printable Ti_3C_2-GO nanocomposites are an excellent sensing platform for electrochemical determination.
 [DOI: 10.1149/2.0051807jes]

Manuscript submitted January 10, 2018; revised manuscript received March 28, 2018. Published April 17, 2018.

MXenes, a new two-dimensional family of metal carbides and/or nitrides,[1–4] inspire enthusiasm for research because they combine hydrophilic surfaces, good structural and chemical stability, excellent electrical conductivity, and environment friendly properties.[5] The formula of MXenes phases is $M_{n+1}X_nT_x$, where M is a transition metal, X is carbon and/or nitrogen, and T_x is surface functionalized. MXene is a younger two-dimensional solid, produced by selectively etching from group A (generally group IIIA and IVA element) layer of the original MAX phases, which comprises a layered, hexagonal early-transition-metal carbides and nitrides[6] family having more than 70 members. To date, all MXenes have been produced by etching the MAX phases in concentrated hydrofluoric acid (HF).[7,8]

MXenes are promising candidates for lithium-ion batteries,[9] supercapacitors,[10] hydrogen storage[11] and adsorption of heavy metals.[12] However, the MXene-Ti_3C_2 of initial formulation[7] lacks stability, which was stable at room temperature for around 1 hour and then completely aggregated at the bottom of the bottle without touch. Because of the low operating concentration and poor stability of the Ti_3C_2 slurry, it is not possible to perform microfabrication and mass production. The utilization of Ti_3C_2 is strictly limited by its processable ability.

Graphene, the latest two-dimensional nanocarbon material, is highly promising for electrochemical biosensing due to its large two-dimensional electrical conductivity, excellent electron transfer rate, huge specific surface area and efficient direct electrochemistry.[13] For solution-processing based applications, graphene oxide (GO), which can be synthesized on a large scale by the modified Hummer's method, can be easily dispersed in water because there are many oxygen-rich functional groups, such as hydroxyl, epoxy, and carboxylic.[14,15] Therefore, GO was selected to modify Ti_3C_2 to improve the stability and electrochemical performance of Ti_3C_2 slurry.

Inkjet printing is a non-contact prototyping technique with highly flexible design, speed and high spatial resolution. Compared with other printing techniques (e.g., screen printing and microcontact printing), inkjet printing has attracted more attention due to its significant advantages involving compatibility with various substrates, availability of non-contact and no-mask patterning, low temperature processing, and no requirement for vacuum processing.[16] To date, as printable conducting inks, a variety of conductive nanomaterials have been successfully inkjet-printed, including silver,[17] copper,[18] and some conductive carbon materials like carbon nanotubes[19] and graphene,[20] which provide the basis for the various applications in the future.

Hydrogen peroxide (H_2O_2), an important chemical material in the medical, chemical and military fields, is a common reactive oxygen species (ROS) in living cells.[21] Therefore, low-cost, rapid and accurate detection of hydrogen peroxide is very important. Many methods are used to detect hydrogen peroxide, such as horseradish peroxidase-based spectrophotometry, titration and electrochemical techniques. At present, electrochemical sensors have been widely used in hydrogen peroxide detection because of their low cost, real-time detection, fast response, high stability, high sensitivity and selectivity.[22] Wang[23] and Liu[24] respectively synthesized the TiO_2-Ti_3C_2 and MoS_2-rGO nanocomposites, which were used to immobilize hemoglobin (Hb) to fabricate a mediator-free biosensor. The prepared nanocomposites greatly enhanced the biological activity of Hb.

In this work, we successfully constructed the inkjet-printed hydrogen peroxide (H_2O_2) sensor by Ti_3C_2-GO nanocomposites, and investigated the electrochemical performance of the Hb/Ti_3C_2-GO/gold foil electrodes toward H_2O_2. As one of the most important kinds of reactive oxygen species (ROS), H_2O_2 plays a key role in the biological system because it can be produced by most of the oxidase reactions.[25] The Ti_3C_2-GO nanocomposites were used for inkjet printing, and the further prepared sensors showed good performance for the detection of H_2O_2 (Fig. 1). Therefore, the present work can provide an effective way to broaden the applications of MXene in electrochemical sensors.

Experimental

Materials and apparatus.—Phosphate buffered saline (PBS) powder was purchased from Sigma-Aldrich. Hemoglobin (Hb) was purchased from Macklin. Unless otherwise noted, other chemicals (analytical grade) in this work were from Aladdin and used as received. In all experiments, deionized water was used.

Scanning electron microscopy (SEM) images were taken by JEOL JSM-7800F, Japan. X-Ray diffraction (XRD) measurements were performed on a Shimadzu diffractometer (XRD-7000, Tokyo, Japan) operating in reflection mode with Cu Kα radiation at a step size of 0.06 per second. The particle sizes of Ti_3C_2 and Ti_3C_2-GO nanodispersion were measured by Malvern Zetasizer Nano-ZS90 (United Kingdom). Atomic force microscope (AFM) images were taken by Bruker Dimension FastScan (USA). The specific surface area (SSA) was obtained using a Brunauer-Emmett-Teller apparatus (BET, Micromeritics, ASAP 2020). The optical microscope images were characterized by Nikon ECLIPSE Ti-S (Japan) inverted microscope. The thickness of the inkjet printing patterns was measured by KOSAKA ET200 (Japan) profilometer.

[z]E-mail: bweng1984@gmail.com; chenjc@swu.edu.cn

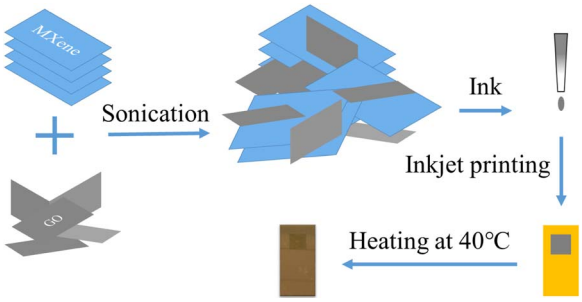

Figure 1. The schematic diagram of the fabrication process of the printed Ti_3C_2-GO nanocomposites on gold foil.

All electrochemical experiments were performed with a CHI 660E electrochemical workstation (CH Instruments, Shanghai, China). A conventional three-electrode system (consisted of a platinum flat (10 mm × 10 mm) as the counter electrode, an Ag/AgCl as the reference electrode and a printed conductive substrate as the working electrode) was used in all electrochemical experiments. Unless otherwise stated, 0.1 M pH 7.0 PBS was used as the supporting electrolyte in all experiments.

Synthesis of Ti_3C_2-GO nanocomposites.—The GO dispersion was prepared using the previously reported modified Hummers' method.[26] Next, the GO dispersion was diluted to 1 $mg \cdot mL^{-1}$ with distilled water.

The original MAX phase, Ti_3AlC_2, was ball milled for 4 h, 8 h and 24 h. The mass ratio of ball to sample was 10:1, and the speed was 450 rpm. The ball milled Ti_3AlC_2 was filtered through a 400 mesh sieve. The treated Ti_3AlC_2 was etched in a mixture of LiF/HCl. 1.98 of g LiF and 30 mL of 6 M HCl were mixed into a PTFE bottle, and the mixture was stirred with a magnetic PTFE stir bar until LiF dissolved. 3 g of treated Ti_3AlC_2 was slowly added into the mixture to avoid a vigorous reaction. The bottle was then covered and immersed in a water bath held at 40°C for 45 h with constant stirring. This solution was washed several times with 40 times distilled water and centrifuged at 7500 rpm for 15 minutes until the supernatant had a pH of approximately 6. The sediment was dispersed in distilled water and sonicated in an ice-water bath for 1 h while continuously bubbled with Ar. After sonication, the aqueous Ti_3C_2 dispersion was centrifuged at 500 rpm for 5 minutes. The supernatant was collected and stored in a refrigerator for the subsequent experiments.

The Ti_3C_2-GO nanocomposites were synthesized by a simple process. The aqueous Ti_3C_2 dispersion was diluted to 1 $mg \cdot mL^{-1}$ with distilled water. 5 mL aqueous Ti_3C_2 dispersion was added to 5 mL GO dispersion (1 $mg \cdot mL^{-1}$) with 20 μL Nafion (0.5%) polymer as binder. The mixture was stirred for 30 minutes and sonicated in an ice-water bath for 30 minutes.

Inkjet printing of the Ti_3C_2-GO nanocomposites.—The Ti_3C_2 nanolayers and Ti_3C_2-GO nanocomposites were independently printed on optical glass and gold foil by inkjet printer Dimatix 2835 (Fujifilm) with 10 pL cartridge and 20 μm drop space. Then, the printed substrates were dried in air for 10 minutes, and placed on a plate heating apparatus at 40°C for 30 minutes. The fabrication process of the printed Ti_3C_2-GO electrode is illustrated in Fig. 1.

For H_2O_2 sensors, 20 μL of 1 $mg \cdot mL^{-1}$ Hb were applied to the surface of Ti_3C_2-GO/gold foil to prepare the Hb/Ti_3C_2-GO/gold foil electrodes and then dried in air. Finally, Nafion (20μL, 0.5%) was dropped on the surface of Hb/Ti_3C_2-GO/gold foil electrodes to form a Nafion membrane.

Prior to printing, the substrates were hydrophilic activated by a UV cleaning machine for 5 minutes.

Electrochemical performance.—Cyclic voltammetry (CV) and differential pulse voltammetry (DPV) of the Hb/Ti_3C_2-GO/gold foil electrodes were carried out with H_2O_2. The various concentrations of H_2O_2 samples were prepared by added H_2O_2 into PBS solution with constant mildly stirring. The selectivity of the Hb/Ti_3C_2-GO/gold foil electrodes was carried out by the DPV curves.

The detection of H_2O_2 in human serum samples was measured by Hb/Ti_3C_2-GO/gold foil electrodes. Human serum samples obtained from local hospital were centrifuged and diluted 10-fold with PBS. DPV curves were measured by continuously adding different concentrations of H_2O_2 to the human serum solution.

Prior to electrochemical measurements, the printed electrodes were activated by CV at a scan rate of 0.1 $V \cdot s^{-1}$ for 20 segments.

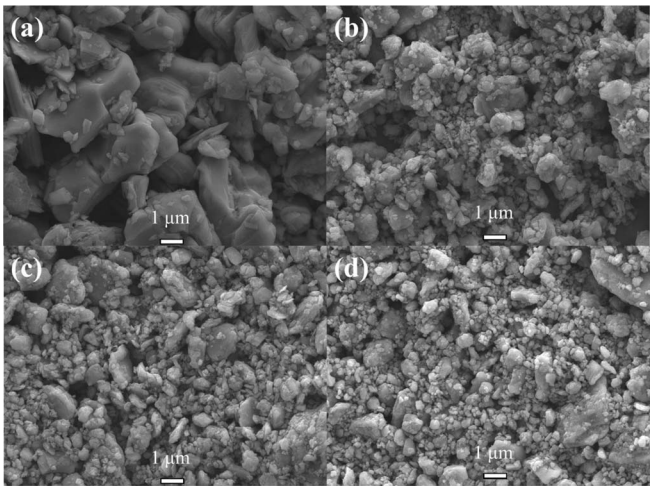

Figure 2. SEM images of original MAX phase Ti_3AlC_2 (a), after 4 h ball milled (b), after 8 h balled milled (c) and after 24 h balled milled (d).

Results and Discussion

The optimization of two-dimensional Ti_3C_2 MXene.—As shown in Fig. 2a, the sizes of Ti_3AlC_2 without ball milled were mainly a few microns. In Figs. 2b, 2d, after ball milled, most of the original MAX phase became smaller and the size was significantly reduced to 1 μm or less. As showed from Fig. 2b, the ball milling was not completely finished after 4 h, since there were some original large particles. After ball milling for 8 h, the MAX phase was further ball milled and its size became smaller (Fig. 2c). Notes that the ball milling has been basically completed at the time. With the extension of milling time to 24h, Fig. 2d showed that there was no significant reduction in size. However, in subsequent experiments, we found that the stability of the Ti_3C_2 slurry after 24 h ball milled became worse, probably because large particles were easier to drag small particles to aggregate. Thus, in order to improve the stability of Ti_3C_2 slurry, it is necessary to reduce its concentration, but this is not conducive to practical application. In addition, some large particles still exist in all ball milled samples, as some samples at the bottom of the ball mill bottle were not completely ball milled because the ball mill rotated horizontally and the bottom of the ball mill bottle was not flat.

In general, after 8 h ball milled, the ball milling level is more appropriate. The Ti_3C_2 slurry after 8 h ball milled was stable at room temperature for around 3 h and in the refrigerator for 6–8 h. It can be concluded that the ball milling can obviously reduce the particle size of the Ti_3C_2 slurry to improve its stability. In this experiment, the best ball milling time was 8 h.

Characterization of the Ti_3C_2-GO nanocomposites.—As shown in Figs. 3a, 3b, the large original MAX phase particles were etched and exfoliated, and the ball milled small particles become to a few layers flakes which interspersed the large particles. The as-synthesized Ti_3C_2 possesses the organ-like structure with one end closing of the Ti_3C_2 nanolayers and the other end opening of that.[27] It has a layered

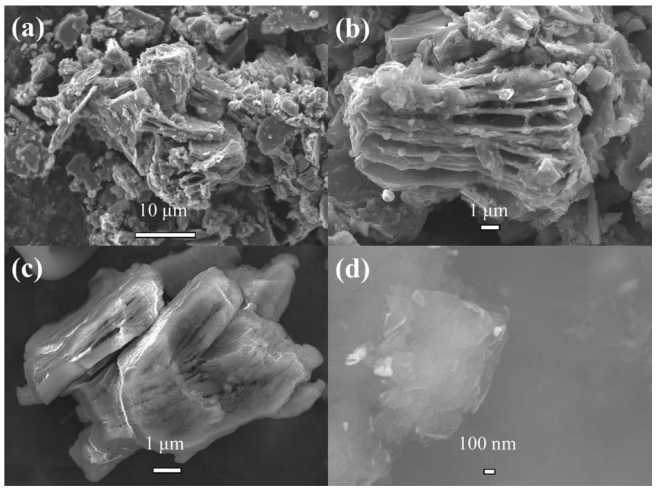

Figure 3. SEM images of Ti_3C_2 (a, b) and Ti_3C_2-GO (c, d).

morphology resembling exfoliated graphite.[28] In order to further improve the stability of Ti_3C_2 for inkjet printing and H_2O_2 sensor, GO was selected to modify Ti_3C_2 to improve the stability and electrochemical performance of Ti_3C_2 slurry. GO modified MXene can form stable dispersions that can last at room temperature for 24 h and in a refrigerator for several days. After modification, Figs. 3c, 3d showed that GO was covered and embedded in Ti_3C_2 to form a stable nanocomposites structure, which was important for its stability and electrical conductivity. Moreover, due to the high surface area of Ti_3C_2-GO (approximately 58.425 $m^2 \cdot g^{-1}$, in Fig. S1) and a large number of small flakes, the effective surface area of Hb/Ti_3C_2-GO/gold foil electrodes was greatly improved.

Fig. 4 presented the XRD patterns of Ti_3AlC_2, Ti_3C_2, GO and Ti_3C_2-GO nanocomposites, respectively. By comparison with Ti_3AlC_2, it can be seen that, from the XRD patterns of the HF-etched Ti_3C_2, the strongestpeak at 39° disappears, which indicates the transformation from Ti_3AlC_2 to $Ti_3C_2T_x$.[29] In addition, the (00l) peaks of $Ti_3C_2T_x$, such as (002) and (006), were broadened, lost intensity, and shifted to lower angles compared to their location before treatment, indicating the increase of intersheet spacing, which demonstrated that Al was replaced by -OH, -F and/or =O. The XRD pattern of Ti_3C_2-GO nanocomposites showed the same diffraction peaks as Ti_3C_2 and GO, confirming the coexistence of Ti_3C_2 nanolayers and GO in the nanocomposites.

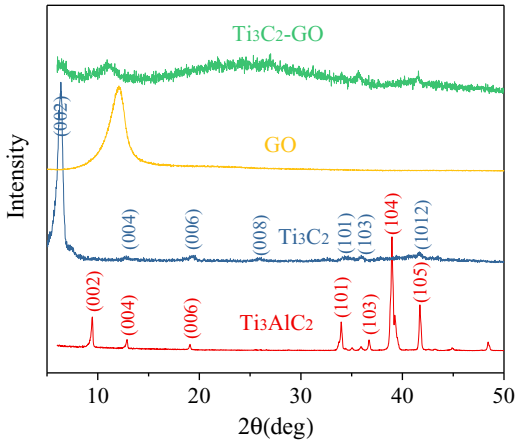

Figure 4. XRD patterns of Ti_3AlC_2, Ti_3C_2, GO and Ti_3C_2-GO nanocomposites.

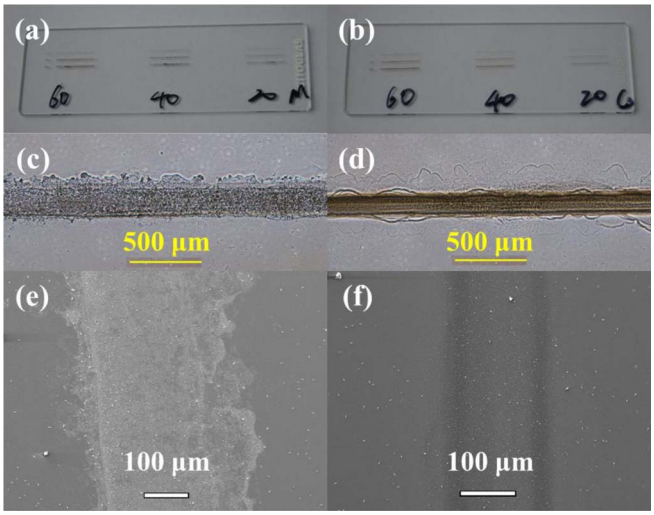

Figure 5. Digital image of Ti_3C_2 (a) and Ti_3C_2-GO (b) on optical glass. Optical microscope images of printed trace of Ti_3C_2 (c) and Ti_3C_2-GO (d). SEM images of printed trace of Ti_3C_2 (e) and Ti_3C_2-GO (f).

The physical sizes of Ti_3C_2-GO nanodispersion have been characterized by dynamic light scattering (DLS) illustrated (Fig. S2). The particle sizes of Ti_3C_2, GO and Ti_3C_2-GO were approximately 70 nm, 80 nm and 100 nm, respectively. All of the particle sizes were nanoscale, and Ti_3C_2-GO was slightly bigger than Ti_3C_2 and GO, confirming that GO has excellently modified Ti_3C_2. This not only improved the stability of Ti_3C_2, but also was very important for its printability.

Inkjet printing of the Ti_3C_2-GO nanocomposites.—The Ti_3C_2 nanolayers and Ti_3C_2-GO nanocomposites were printed on optical glass according to the different number of layers and lines, respectively. Figs. 5a, 5b showed that all the printed patterns had good results, and as the number of layers and lines increased, it became clearer, confirming that Ti_3C_2 nanolayers and Ti_3C_2-GO nanocomposites were printable. The printed patterns were further characterized by a microscope in Figs. 5c, 5d. The printed traces of Ti_3C_2-GO nanocomposites were narrower, clearer and more uniform than Ti_3C_2, which demonstrated that its printability has been improved. The SEM image (Figs. 5e, 5f) revealed that the diffusivity of the Ti_3C_2-GO nanocomposites was significantly lower than that of Ti_3C_2, which was very important for printing a particular pattern. Table S1 showed the thickness of the printed patterns. The average thicknesses of Ti_3C_2 nanolayers and Ti_3C_2-GO nanocomposites were 349.5 nm and 231.7 nm, respectively, indicating that Ti_3C_2-GO nanocomposites were better than pure Ti_3C_2 nanolayers and more conducive to printing specific patterns.

Fig. 6 showed the AFM images of Ti_3C_2 and Ti_3C_2-GO printed patterns. In Figs. 6a, 6b, both printed patterns obviously exhibited a large number of layered morphology, which was very important for its electrochemical performance. Even after the GO was introduced, the Ti_3C_2 nanolayers retained its original morphology as GO particles were covered and embedded in the Ti_3C_2 to form a stable nanocomposites film.[30] As shown in Figs. 6c, 6d, the 3D images provided a better understanding of the morphology of Ti_3C_2 nanolayers and Ti_3C_2-GO nanocomposites. The Ti_3C_2-GO nanocomposites were significantly more uniform than Ti_3C_2 nanolayers. This demonstrated that GO has been modified on the surface of the Ti_3C_2 nanolayers successfully and improved its printing performance.

Electrochemical characteristics.—The Ti_3C_2-GO nanocomposites were printed on a conductive substrate (gold foil) and further used to prepare the electrode for electrochemical detection. The Hb was applied to the surface of Ti_3C_2-GO/gold foil electrodes to prepare the Hb/Ti_3C_2-GO/gold foil electrodes for the detection of H_2O_2.

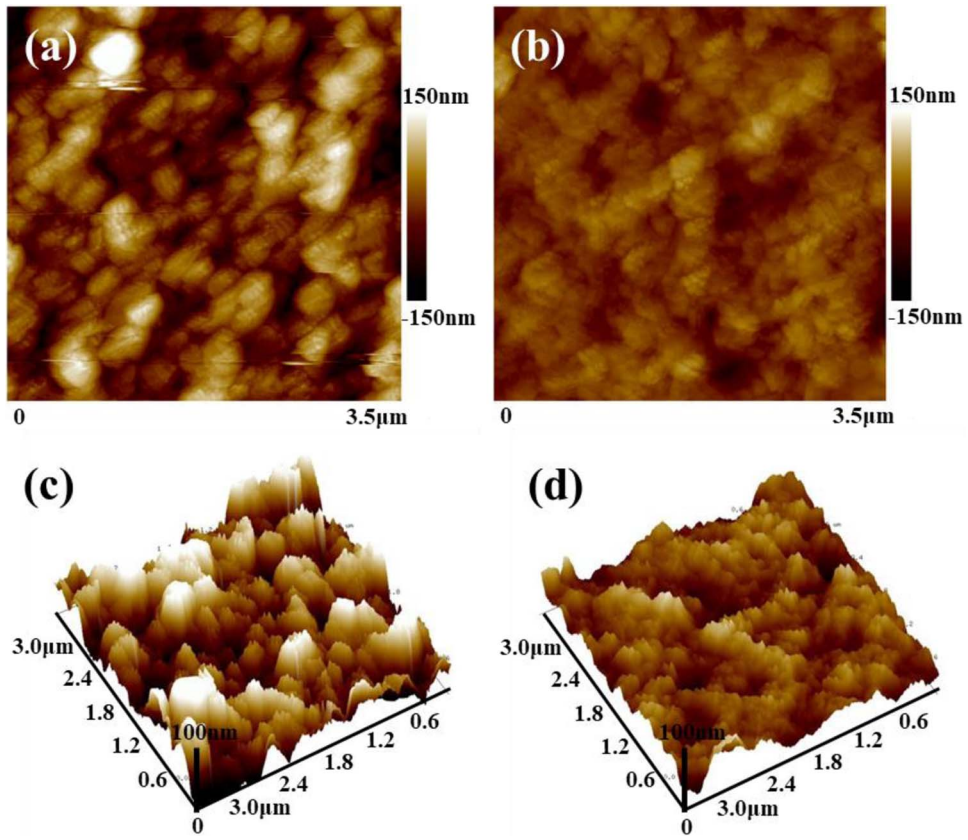

Figure 6. AFM image of printed patterns of Ti_3C_2 (a), Ti_3C_2 -GO (b), and (c, d) image corresponding to the 3D morphologies.

Fig. 7a showed the CV curves of different electrodes at a scan rate of 0.1 $V \cdot s^{-1}$ in 0.1 M pH 7.0 PBS with 100μM H_2O_2. There was no obvious chemical reaction of H_2O_2 on Ti_3C_2-GO/gold foil electrodes, indicating that the electrode was electrochemical inactive toward H_2O_2. The Hb/gold foil electrodes exhibited a couple of stable and well-defined redox peak at −0.2 V and 0 V vs. Ag/AgCl, which demonstrated that the Hb/gold foil electrodes were electroactive well for H_2O_2 at the electrochemical system. Compared with Hb/gold foil electrodes, the Hb/Ti_3C_2-GO/gold foil electrodes significantly promoted the redox reaction. It can be concluded that Ti_3C_2-GO nanocomposites can promote the electron transfer better, which may be due to its special structure and performance.

As shown in Fig. S3, the optimization of the Hb/Ti_3C_2-GO/gold foil electrodes were investigated. In Fig. S3(a), the effect of pH value on the electrochemical behavior of the Hb/Ti_3C_2-GO/gold foil electrodes were studied. The electrodes were in solutions at different pH values and the strongest peak current response was observed at pH 7.0 for H_2O_2 detection. The mass ratio of Ti_3C_2 to GO in Ti_3C_2-GO nanocomposites was investigated by DPV curves (Fig. S3b). When the mass ratio of Ti_3C_2 to GO nanoparticles changed to 4:6, the peak current reached its maximum value.

In Fig. 7b, with the increase of the concentrations of H_2O_2, the DPV curves sharply increased at −0.08 V, which confirmed that Hb/Ti_3C_2-GO/gold foil electrodes contributed significantly to the electrochemical detection of H_2O_2. The linear relationship between the peak current and the logarithm of H_2O_2 concentration can be seen in Fig. 7c, which showed a line linear equation: $I_p = 6.20\lg c + 42.27$ ($R^2 = 0.9987$), a dynamic range from 2 μM to 1 mM, and a detection limit of 1.95 μM (based on the blank and 3SD). The results showed that the Hb/Ti_3C_2-GO/gold foil electrodes could maintain the biological activity of Hb and detect H_2O_2 by DPV means.

To evaluate the practical applicability of the H_2O_2 sensors, H_2O_2 assays were performed in human serum samples, in Table S2. The human serum samples were purified by centrifugation and diluted 10-fold with PBS. The relative standard deviation of the three measurements was less than 4.48%, indicating that the H_2O_2 sensor has excellent accuracy and repeatability and can be used in practical samples.

The selectivity of the sensors was determined by the eight common interfering substances such as glucose (Glu), ascorbic acid (AA), citric acid (CA), dopamine (DA), acetic acid (HAc), oxalic acid(OA), 4-acetamidophenol(APAP) and uric acid (UA) through the DPV curves. As Fig. 7d shown, compared with H_2O_2, there was no obvious response to these interfering substances, which may be attributed to the intrinsic selectivity of the Hb/Ti_3C_2-GO/gold foil electrodes to its substances.

Conclusions

The Ti_3C_2 was successfully prepared by simply etching Al from Ti_3AlC_2. Because of the poor stability of Ti_3C_2 slurry, ball milling and GO were used to improve its stability and performance. Then we applied inkjet printing technology to fabricate a printed Ti_3C_2-GO electrode for H_2O_2 biosensor. During electrochemical characterizations, the Hb/Ti_3C_2-GO/gold foil electrodes displayed a detection limit of 1.95 μM and a dynamic linear range from 2 μM to 1 mM for H_2O_2. The printed sensors also showed excellent performance in human serum samples. These results demonstrated that the Ti_3C_2-GO nanocomposites were suitable for inkjet printing and provided the low-cost and environmental friendly, highly stable and better performing sensing electrodes for various applications.

Acknowledgments

We gratefully acknowledge to the financial support by the China Postdoctoral Science Foundation (2016M602627), Chongqing Postdoctoral Science Special Foundation (Xm2016032), Transformative Project for Excellent Scientific and Technological Achievements

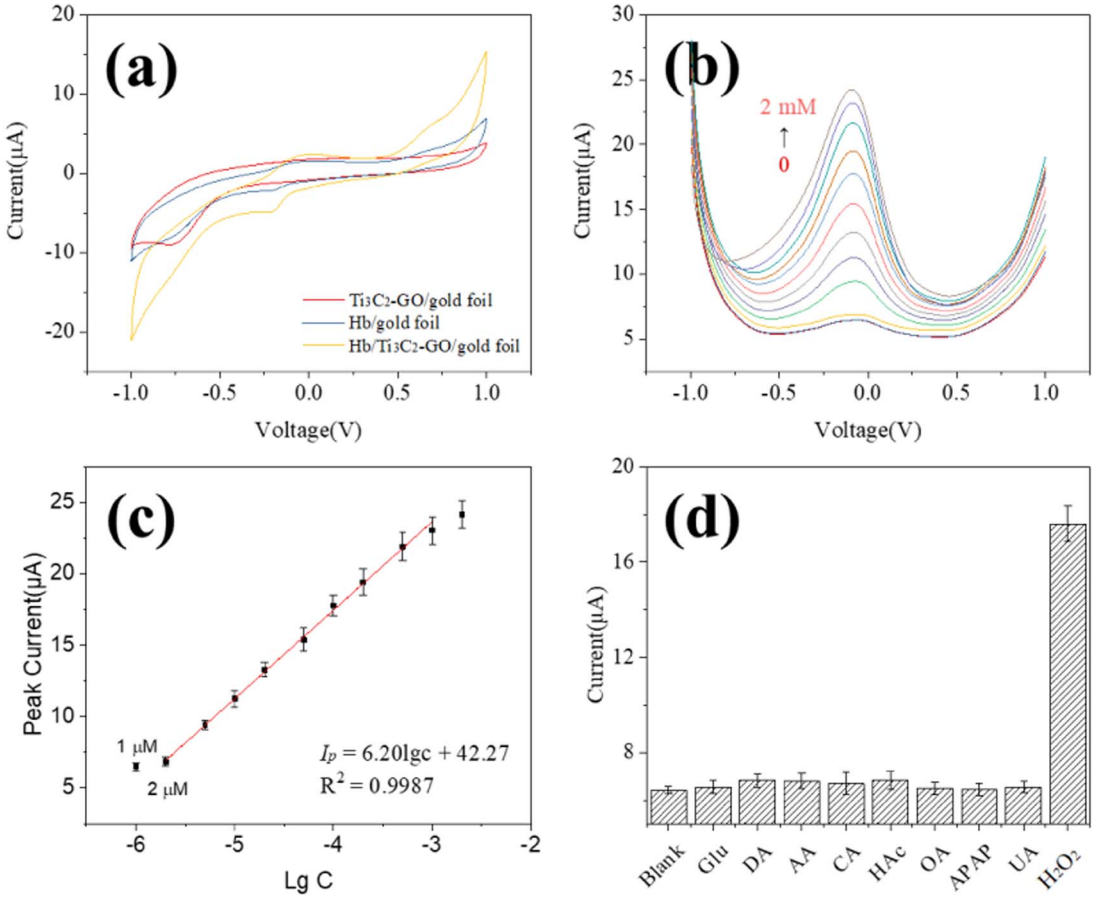

Figure 7. (a) CV curves of Ti_3C_2-GO/gold foil electrodes, Hb/gold foil electrodes and Hb/Ti_3C_2-GO/gold foil electrodes at a scan rate of 0.1 $V \cdot s^{-1}$ in 0.1 M pH 7.0 PBS with 100μM H_2O_2. (b) DPV curves of Hb/Ti_3C_2-GO/gold foil electrodes in stirred 0.1 M pH 7.0 PBS containing 0 μM, 1 μM, 2 μM, 5 μM, 10 μM, 20 μM, 50 μM, 100 μM, 200 μM, 500 μM, 1 mM, and 2 mM H_2O_2. (c) The linear relationship between the peak current and the logarithm of H_2O_2 concentration. (d) Peak current of DPV curves of Hb/Ti_3C_2-GO/gold foil electrodes to addition of 0.1mM Glu, 0.01 mM DA, 0.1 mM AA, 0.1 mM CA, 0.1 mM HAc, 0.1 mM OA, 0.1 mM APAP, 0.1 mM UA and 0.1 mM H_2O_2 in 0.1 M pH 7.0 PBS, respectively.

in University (KJZH17108), Special Program for Chongqing Social Business and People's Livelihood Guarantee of Science and Technology (cstc2017shmsA30001) and Science Foundation for Youths of Science and Technology Department of Shaanxi Province (2016JQ2026) and Foundation for High-level Talents of Ankang University (2014AYQDZR04).

ORCID

Jiucun Chen https://orcid.org/0000-0002-6677-2228

References

1. O. Mashtalir, M. Naguib, V. N. Mochalin, Y. Dall'Agnese, M. Heon, M. W. Barsoum, and Y. Gogotsi, *Nature communications*, **4**, 1716 (2013).
2. M. R. Lukatskaya, O. Mashtalir, C. E. Ren, Y. Dall'Agnese, P. Rozier, P. L. Taberna, M. Naguib, P. Simon, M. W. Barsoum, and Y. Gogotsi, *Science*, **341**, 1502 (2013).
3. M. Khazaei, M. Arai, T. Sasaki, C.-Y. Chung, N. S. Venkataramanan, M. Estili, Y. Sakka, and Y. Kawazoe, *Advanced Functional Materials*, **23**, 2185 (2013).
4. M. Naguib, O. Mashtalir, J. Carle, V. Presser, J. Lu, L. Hultman, Y. Gogotsi, and M. W. Barsoum, *ACS nano*, **6**, 1322 (2012).
5. Q. Peng, J. Guo, Q. Zhang, J. Xiang, B. Liu, A. Zhou, R. Liu, and Y. Tian, *Journal of the American Chemical Society*, **136**, 4113 (2014).
6. M. W. Barsoum, *MAX phases: properties of machinable ternary carbides and nitrides*, John Wiley & Sons, 2013.
7. M. Ghidiu, M. R. Lukatskaya, M.-Q. Zhao, Y. Gogotsi, and M. W. Barsoum, *Nature*, **516**, 78 (2014).
8. O. Mashtalir, M. Naguib, B. Dyatkin, Y. Gogotsi, and M. W. Barsoum, *Materials Chemistry and Physics*, **139**, 147 (2013).
9. Q. Tang, Z. Zhou, and P. Shen, *Journal of the American Chemical Society*, **134**, 16909 (2012).
10. X. Yang, C. Cheng, Y. Wang, L. Qiu, and D. Li, *science*, **341**, 534 (2013).
11. Q. Hu, D. Sun, Q. Wu, H. Wang, L. Wang, B. Liu, A. Zhou, and J. He, *The Journal of Physical Chemistry A*, **117**, 14253 (2013).
12. M. Hua, S. Zhang, B. Pan, W. Zhang, L. Lv, and Q. Zhang, *Journal of Hazardous Materials*, **211**, 317 (2012).
13. S. Mao, K. Yu, G. Lu, and J. Chen, *Nano Research*, **4**, 921 (2011).
14. S. Wang, P. K. Ang, Z. Wang, A. L. L. Tang, J. T. L. Thong, and K. P. Loh, *Nano Letters*, **10**, 92 (2010).
15. V. Dua, S. P. Surwade, S. Ammu, S. R. Agnihotra, S. Jain, K. E. Roberts, S. Park, R. S. Ruoff, and S. K. Manohar, *Angewandte Chemie-International Edition*, **49**, 2154 (2010).
16. L. Huang, Y. Huang, J. Liang, X. Wan, and Y. Chen, *Nano Research*, **4**, 675 (2011).
17. M. Layani, M. Grouchko, S. Shemesh, and S. Magdassi, *Journal Of Materials Chemistry*, **22**, 14349 (2012).
18. D. Deng, Y. Jin, Y. Cheng, T. Qi, and F. Xiao, *Acs Applied Materials & Interfaces*, **5**, 3839 (2013).
19. A. Shimoni, S. Azoubel, and S. Magdassi, *Nanoscale*, **6**, 11084 (2014).
20. K.-Y. Shin, J.-Y. Hong, and J. Jang, *Advanced materials*, **23**, 2113 (2011).
21. M. Sawangphruk, Y. Sanguansak, A. Krittayavathananon, S. Luanwuthi, P. Srimuk, S. Nilmoung, S. Maensiri, W. Meevasana, and J. Limtrakul, *Carbon*, **70**, 287 (2014).
22. C. Wang, X. Zou, Q. Wang, K. Shi, J. Tan, X. Zhao, Y. Chai, and R. Yuan, *Analytical Methods*, **6**, 758 (2014).
23. F. Wang, C. Yang, M. Duan, Y. Tang, and J. Zhu, *Biosensors & bioelectronics*, **74**, 1022 (2015).
24. H. Liu, X. Chen, X. Su, C. Duan, K. Guo, and Z. Zhu, *Journal of The Electrochemical Society*, **162**, B312 (2015).
25. X. Sun, S. Guo, Y. Liu, and S. Sun, *Nano Letters*, **12**, 4859 (2012).
26. D. C. Marcano, D. V. Kosynkin, J. M. Berlin, A. Sinitskii, Z. Sun, A. Slesarev, L. B. Alemany, W. Lu, and J. M. Tour, *ACS nano*, **4**, 4806 (2010).
27. F. Wang, C. Yang, C. Duan, D. Xiao, Y. Tang, and J. Zhu, *Journal of The Electrochemical Society*, **162**, B16 (2015).
28. X. Li, X. Wang, L. Zhang, S. Lee, and H. Dai, *Science*, **319**, 1229 (2008).
29. F. Chang, C. Li, J. Yang, H. Tang, and M. Xue, *Materials Letters*, **109**, 295 (2013).
30. V. Nicolosi, M. Chhowalla, M. G. Kanatzidis, M. S. Strano, and J. N. Coleman, *Science*, **340**, 1226419 (2013).